Journal of Materials Chemistry A

Accepted Manuscript

This is an *Accepted Manuscript*, which has been through the Royal Society of Chemistry peer review process and has been accepted for publication.

Accepted Manuscripts are published online shortly after acceptance, before technical editing, formatting and proof reading. Using this free service, authors can make their results available to the community, in citable form, before we publish the edited article. We will replace this *Accepted Manuscript* with the edited and formatted *Advance Article* as soon as it is available.

You can find more information about *Accepted Manuscripts* in the Information for Authors.

Please note that technical editing may introduce minor changes to the text and/or graphics, which may alter content. The journal's standard Terms & Conditions and the Ethical guidelines still apply. In no event shall the Royal Society of Chemistry be held responsible for any errors or omissions in this *Accepted Manuscript* or any consequences arising from the use of any information it contains.

ROYAL SOCIETY OF CHEMISTRY

www.rsc.org/materialsA

Journal of Materials Chemistry A

COMMUNICATION

Compositionally-Tunable Mechanochemical Synthesis of $Zn_xCo_{3-x}O_4$ Nanoparticles for Mesoporous p-Type Photocathodes

Received 00th January 20xx,
Accepted 00th January 20xx

DOI: 10.1039/x0xx00000x

www.rsc.org/

Shannon. M. McCullough,[a] Cory. J. Flynn,[a] Candy C. Mercado,[b] Arthur J. Nozik,[b,c] and James F. Cahoon[a]

A solid-state mechanochemical synthesis of $Zn_xCo_{3-x}O_4$ was developed with highly tunable Zn concentration. Photovoltaic performance was evaluated in dye-sensitized solar cells and tested with various Zn concentrations, exhibiting maximum performance with $ZnCo_2O_4$. Oxidative treatments led to a nearly three-fold increase in dye loading and a significant increase in short-circuit current density.

A key challenge facing the modern world lies in the development and implementation environmentally-friendly energy sources. Mesoporous dye-sensitized solar cells (DSSCs) have been extensively studied since their first report in 1991.[1] The highest performing DSSCs in the literature feature power conversion efficiencies exceeding 12% and use an n-type TiO_2 photoanode as the working electrode.[2] Analogous p-type DSSCs can, in principle, achieve comparable efficiencies with the circuit operating in reverse by replacing the photoanode with a photocathode. However, the current efficiency record is 2.55% using NiO, the champion photocathode material to-date.[3] The underperformance of NiO compared to TiO_2 demands the investigation of alternate materials, which is an active area of research including, for instance, efforts to develop $Ni_xCo_{3-x}O_4$ and Cu(I) delafossites.[4–9]

A DSSC is a solar-to-electric photovoltaic device that typically features one photoactive electrode, either an n-type anode or a p-type cathode, and one dark counter electrode, typically Pt. In a tandem configuration, however, the anode and cathode are placed in series and both are photoactive, allowing for a larger photovoltage and complementary light absorbance, with the photoanode absorbing blue wavelengths and the photocathode absorbing red wavelengths. Targeting a tandem design enables the use of photocathode materials with band gaps as small as ~2 eV, which would typically not be considered for a conventional DSSC. Moreover, tandem solar fuel devices, such as dye-sensitized photoelectrosynthesis cells (DSPECs),[10] can synthesize solar fuels by integrating molecular catalysts that store solar energy in a chemical bond. With current materials, the photocathode significantly limits the performance of a DSPEC or similar tandem device, further motivating interest in identifying new materials.[10–15]

$ZnCo_2O_4$ is a candidate p-type semiconductor that crystallizes in the cubic spinel lattice.[16–18] The general spinel formula, AB_2O_4, features a divalent metal, A, tetrahedrally coordinated to oxygen, and a trivalent metal, B, octahedrally coordinated to oxygen. For example, Co_3O_4 is a spinel, consisting of one Co^{2+} and two Co^{3+}. $ZnCo_2O_4$ can be considered a substituted Co_3O_4 material, where Zn^{2+} replace the Co^{2+} cations. The Zn^{2+} substitution results in a change in several material properties that are beneficial to p-type DSSCs, including increasing the optical band gap, conductivity, doping level, and hole mobility.[17,18] A dense thin-film of $ZnCo_2O_4$ has previously been reported in a DSSC configuration.[16] However, a high surface area mesoscale form is critical for increasing the light-harvesting efficiency of $ZnCo_2O_4$. Nanostructures of $ZnCo_2O_4$ have been reported for applications in catalysis and batteries.[19–25] Here, we present a novel solid-state synthesis of phase-pure $Zn_xCo_{3-x}O_4$ nanoparticles with highly tunable Zn stoichiometry, and we present the first report of p-type DSSCs using mesoscopic $Zn_xCo_{3-x}O_4$ films.

$Zn_xCo_{3-x}O_4$ spherical nanoparticles were synthesized via a mechanochemical solid-state preparation. Typical mechano-chemical syntheses require high levels of mechanical energy introduced via ball milling over several hours.[26,27] In contrast, the preparation developed here is a highly facile, low-energy reaction using manual grinding of $Co(NO_3)_2{\cdot}6H_2O$, $Zn(NO_3)_2{\cdot}6H_2O$ and NaOH to form a mixed metal hydroxide of general formula $Zn_xCo_{3-x}(OH)_6$, as shown in Figure 1A. Upon calcination at temperatures ranging from 300 to 500 °C, a phase-pure spinel is observed. An advantage of this synthesis is that by simply tuning the starting ratio of cobalt and zinc

[a] Department of Chemistry, University of North Carolina at Chapel Hill, Chapel Hill, NC 27599-3290, United States.
[b] Renewable and Sustainable Energy Institute, and Department of Chemistry and Biochemistry, University of Colorado, Boulder, CO 80309-0027, United States.
[c] National Renewable Energy Laboratory, 15013 Denver West Parkway, Golden, CO 80401, United States.

Electronic Supplementary Information (ESI) available: Experimental details, supporting figures and table. See DOI: 10.1039/x0xx00000x

Journal of Materials Chemistry A Accepted Manuscript

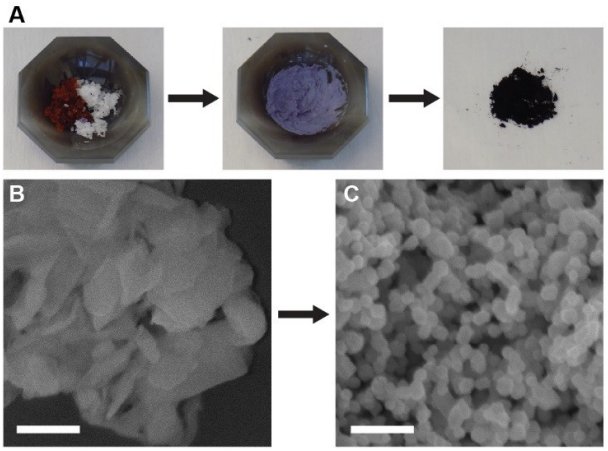

Figure 1. Mechanochemical synthesis. (A) Optical images of solid-state nanoparticle synthesis of $Zn_xCo_{3-x}O_4$, showing conversion of the metal salts (left) to the mixed metal hydroxide (middle) and finally the metal oxide (right). (B and C) SEM images of $ZnCo_2(OH)_6$ nanosheets (panel B) and $ZnCo_2O_4$ nanoparticles (panel C). Scale bars, 100 nm.

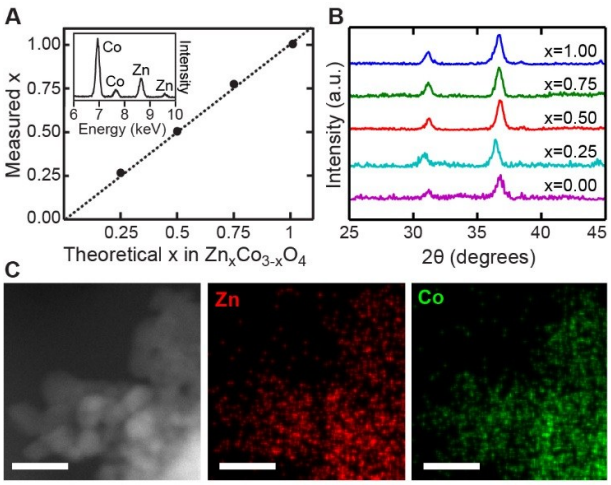

Figure 2. Chemical composition. (A) Zn stoichiometry as measured by EDS. Inset: EDS spectrum of $ZnCo_2O_4$. (B) PXRD patterns for all Zn stoichiometries of $Zn_xCo_{3-x}O_4$. (C) STEM image (left) and EDS maps of Zn (middle) and Co (right). Scale bars, 20 nm.

nitrates, the Zn concentration in the spinel lattice is directly tuned. Five Zn concentrations were studied, where x = 0, 0.25, 0.5, 0.75, and 1, given the general formula, $Zn_xCo_{3-x}O_4$.The morphology of the hydroxide and calcined oxide are confirmed via scanning electron microscopy (SEM) imaging, and the oxide forms nanospheres of 24 ± 5 nm diameter, as shown in Figure 1B-C. The nanospheres form because of the significant change in density between the oxide (6.11 g·cm^{-1}) and the hydroxide (3.60 g·cm^{-1}).[28]

Elemental composition of $Zn_xCo_{3-x}O_4$ was analyzed via energy-dispersive x-ray spectroscopy (EDS), confirming that the Zn concentration is unchanged throughout the synthesis (Figure 2A) and is facilely adjusted within the range of x = 0 to x = 1. Prior to calcination, any unreacted material is rinsed away with H_2O. The synthetic preparation is described in detail in the electronic supplementary information (ESI). Powder x-ray diffraction (PXRD) patterns (Figure 2B) show peaks consistent with spinel lattice. Notably, no peaks characteristic of a wurtzite phase are present in any sample, indicating the absence of ZnO. X-ray photoelectron spectroscopy confirms the presence of Zn^{2+} and Co^{3+} (Figure S1). To characterize the uniformity of Zn within the nanoparticles, EDS mapping in a scanning transmission electron microscope (STEM) was performed, confirming a homogeneous composition in the material (Figure 2C).

The $Zn_xCo_{3-x}O_4$ nanoparticles were processed into thin films on glass slides by spin casting pastes prepared by a modification of literature procedures[29] (see ESI). As shown in Figure 3A, the films are black, and absorbance spectra show increasing absorbance in the 300-500 nm range with increasing Zn concentration. Non-band gap absorbance, likely due to trap states, causes the black appearance, and future optimization will need to address these detrimental trap states. Tauc plots (Figure S2) were used to determine the band gaps, as shown in Figure 3B, for each Zn stoichiometry. As the Zn concentration increases, the band gap also increases. The band gap of $ZnCo_2O_4$ is 2.17 eV, which agrees well with the literature value of 2.2 eV.[17] With decreasing Zn concentration, the optical band gap decreases to a value of 1.85 eV for Co_3O_4, also in agreement with literature values of 1.8 eV.[30]

We probed the electrical transport characteristics of $Zn_xCo_{3-x}O_4$ by measuring the conductivity and doping level of thin films (Figure 4A). Conductance measurements performed with micron-scale electrodes (Figure S3) indicate that the conductivity increases by two orders of magnitude with increasing Zn concentration. Mott-Schottky analysis (Figure S4) yielded the doping level and valence band edge of each stoichiometry of $Zn_xCo_{3-x}O_4$. The doping concentration (Figure 4A) increased by more than one order of magnitude as the Zn substitution increased. This increase most likely results either from an increase in cation vacancies or an increase in the divalent metal (Zn^{2+}) occupying a trivalent site (Co^{3+}), consistent with previous reports.[17,18,31] The electrical mobility of $Zn_xCo_{3-x}O_4$ (Figure 4B) was determined from the conductivity and doping level and shows an increase of more than one order of magnitude with increasing Zn concentration. The values range from a low of 2.41 x 10^{-5} cm^2·V^{-1}·s^{-1} for x = 0 to a maximum of 3.58 x 10^{-4} cm^2·V^{-1}·s^{-1} for x = 0.75. The measured

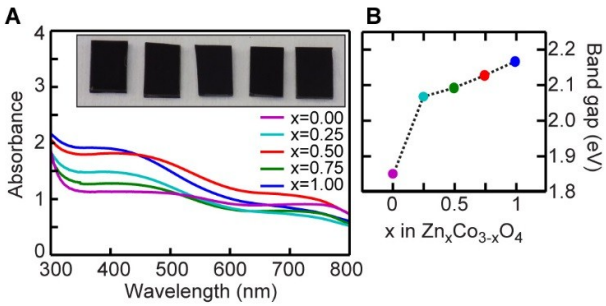

Figure 3. Optical properties. (A) Absorbance spectra of $Zn_xCo_{3-x}O_4$ with various stoichiometries. Inset: photograph of 1.2 µm-thick films with Zn stoichiometries from left to right: x = 0, 0.25, 0.50, 0.75, 1. (B) Band gap of various stoichiometries.

Journal of Materials Chemistry A Accepted Manuscript

This journal is © The Royal Society of Chemistry 20xx

Please do not adjust margins

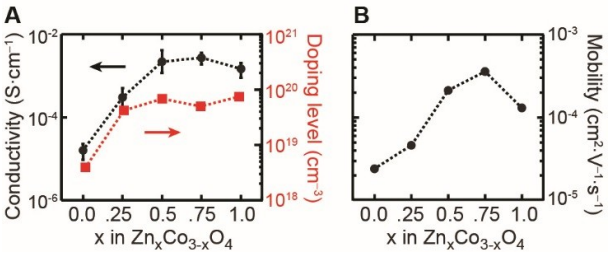

Figure 4. Electrical transport properties. (A) Conductivity (black circles and left-hand axis) and doping level (red squares and right-hand axis) as a function of Zn stoichiometry. (B) Electrical mobility as a function of Zn stoichiometry.

mobility value for Co_3O_4 is on the same order-of-magnitude as literature values,[32,33] and the mobility of the mesoscopic $ZnCo_2O_4$ is approximately two orders of magnitude lower than the previously-reported dense thin film.[16] The difference can be attributed to interparticle hopping required for charge transport in the nanoparticle film. Compared to previous reports on NiO mesoporous films, mobility values of holes in $Zn_xCo_{3-x}O_4$ are comparable given similar annealing conditions.[34] To confirm conduction by holes and thus the p-type nature of the material, the Fermi level was measured via ultraviolet photoelectron spectroscopy (Figure S5), showing that the Fermi level is within 500 meV of the valence band edge. In addition, the Seebeck coefficient of $ZnCo_2O_4$ was measured to be a positive 8050 ± 10 $V \cdot K^{-1}$ (Figure S6).

DSSCs were fabricated to probe how the $Zn_xCo_{3-x}O_4$ thin films perform as mesoscopic hole-conducting photocathodes. Devices with all five Zn concentrations were prepared using 1.2 µm-thick films, the P1 molecular chromophore, and an I^-/I_3^- electrolyte. Full experimental conditions are described in the ESI. Current density-voltage (*J-V*) characteristics were collected in the dark and under AM1.5G one-sun illumination. *J-V* curves are plotted in Figure 5A for all Zn concentrations. Full metrics are provided in the ESI in Table S1. With increasing Zn substitution in the spinel lattice, the short-circuit current density (J_{sc}) increased significantly, ranging from 0.11 ± 0.02 $mA \cdot cm^{-2}$ to 0.37 ± 0.09 $mA \cdot cm^{-2}$ for Co_3O_4 and $ZnCo_2O_4$, respectively (Figure 5B). We attribute the increase in current to the substantial increase in mobility. Absorption spectroscopy (Figure S7) confirmed that the dye-loading on all samples was the same (Figure 5B), and, therefore, not the cause for an increase in J_{sc}. Methods used to quantify dye-loading are described in the ESI. The incident photon-to-current conversion effiency was measured (Figure S8), confirming that the dye generates the photocurrent.

Further material and device optimization was pursued on the highest performing Zn concentration, $ZnCo_2O_4$. Poor dye-loading relative to other metal oxides was identified as a performance limiter.[35] Consequently, we attempted to increase dye-loading by increasing the oxygen concentration on $ZnCo_2O_4$'s surface because P1 features a carboxylic acid linker group that requires a surface oxygen to bind to the metal oxide.[36] It is possible for the surface to be metal-terminated as a result of carbothermal reduction, which can occur in the presence of the polymer, hydroxypropyl cellulose (HPC), used to process the nanoparticles into a paste for spin casting. Annealing the spin-cast films at sufficiently high temperatures (≥300 °C) in air results in a combustion reaction of the HPC, leaving behind the mesoporous metal oxide thin films. These conditions are also favorable for a carbothermal reduction because of the presence of hydrocarbons, oxygen, and sufficiently high temperatures.[37] Although these processing conditions are standard for n-type DSSCs, TiO_2, an exceptionally stable metal oxide, is unlikely to undergo carbothermal reduction.[37,38] Consequently, methods used for n-type DSSCs cannot necessarily be translated to p-type DSSCs, and separate methods will often need to be developed.

Operating under the hypothesis that dye-loading would improve with increased surface oxygen, we pursued alternate strategies to produce a mesoscopic thin film of $ZnCo_2O_4$. The films were treated in an oxidizing environment using an ultraviolet/ozone (UVO) system. The UVO treatment allows for the HPC removal at lower temperatures via alternate reaction mechanisms, producing a mesoporous thin film while preventing carbothermal reduction and maintaining the oxygen-terminated surface. When the films were treated only at 200 °C under UVO atmosphere (condition 2), a nearly three-fold increase in dye-loading, from 8.8 to 23 $nmol \cdot cm^{-3}$, was observed compared to films annealed in air at 300 °C. UVO-treated films were then tested in a DSSC configuration.

Figure 5C illustrates the changes in photocurrent and dye-loading with successive annealing treatments. Although the UVO treated films (condition 2) featured higher dye-loading, the J_{sc} decreased by 21% to 0.26 ± 0.04 $mA \cdot cm^{-2}$. We hypothesized that the low-temperature UVO treatment preserved the oxygen-terminated surface advantageous for dye-loading but was insufficient to sinter the individual nanoparticles together to create an electrically interconnected, mesoporous scaffold. By combining the two annealing techniques, allowing for the UVO removal of the

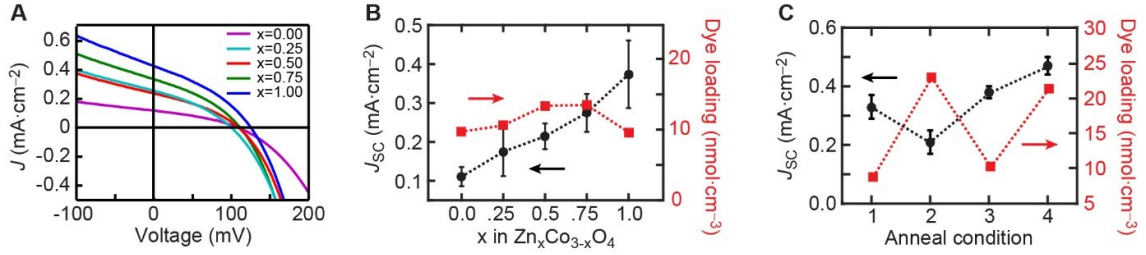

Figure 5. DSSC characterization. (A) *J-V* curves under 1-sun illumination for $Zn_xCo_{3-x}O_4$ of various stoichiometries calcined in air at 300 °C. (B and C) J_{sc} (black circles and left-hand axes) and dye-loading (red squares and right-hand axes) as a function of Zn stoichiometry (panel B) and as a function of annealing condition for $ZnCo_2O_4$ (panel C). In panel C, annealing conditions are 1: air 300 °C; 2: UVO 200°C; 3: UVO 200 °C, air 300 °C; 4: UVO 50 °C; air 300 °C, UVO 200 °C.

Journal of Materials Chemistry A Accepted Manuscript

HPC at low temperatures and electrical sintering of the particles at higher temperatures in air, the J_{sc} improves from 0.26 ± 0.04 mA·cm^{-2} to 0.38 ± 0.02 mA·cm^{-2}. The order of the annealing treatments dictates the device performance. Several conditions were tested, and we report a subset here (Figure 5C) to demonstrate trends. The most successful process (annealing condition 4) results from three successive treatments of the film. First, the HPC is removed via a low-temperature (50 °C) UVO treatment. Second, a high-temperature air anneal at 300 °C electrically sinters the film, and third, a 200 °C UVO treatment increases the oxygen concentration on the surface, which led to the highest J_{sc} of 0.47 ± 0.04 mA·cm^{-2}, a 1-sun power-conversion efficiency of 0.025 %, and a dye loading of 21 nmol·cm^{-2}.

Conclusions

Here, we have presented a solid-state preparation of nanoparticulate $Zn_xCo_{3-x}O_4$ with highly tunable Zn concentration and a pure spinel phase. Tuning the Zn concentration within the spinel lattice improved the electrical properties of the material, significantly increasing the mobility one order of magnitude from ~10^{-5} to ~10^{-4} cm^2·V^{-1}·s^{-1}. The $Zn_xCo_{3-x}O_4$ nanoparticles were processed into a mesoscopic photocathode, which was characterized in a p-type DSSC configuration. Evaluation of DSSC performance with respect to Zn concentration resulted in the trend of increased performance with increased Zn concentration. Through further optimization, UVO treatments on $ZnCo_2O_4$ photocathodes resulted in a nearly threefold increase in dye-loading from 8.8 to 21 nmol·cm^{-3} and an increase J_{sc} from 0.33 ± 0.04 to 0.47 ± 0.04 mA·cm^{-2}. This initial evaluation of $ZnCo_2O_4$ as a mesoporous photocathode demonstrates promise for the further development of this material for solar energy devices.

Acknowledgement

This work was primarily funded by the UNC Energy Frontier Research Center, an EFRC funded by the U.S. Department of Energy, Office of Science, Office of Basic Energy Sciences, under award DE-SC0001011. S.M.M. acknowledges a National Science Foundation graduate research fellowship.

References

1 B. O'Regan and M. Grätzel, *Nature*, 1991, **353**, 737.
2 A. Yella, H. W. Lee, H. N. Tsao, C. Yi, A. K. Chandiran, M. K. Nazeeruddin, E. W. G. Diau, C. Y. Yeh, S. M. Zakeeruddin and M. Gratzel, *Science*, 2011, **334**, 629.
3 I. R. Perera, T. Daeneke, S. Makuta, Z. Yu, Y. Tachibana, A. Mishra, P. Bäuerle, C. A. Ohlin, U. Bach and L. Spiccia, *Angew. Chemie Int. Ed.*, 2015, **54**, 3758.
4 Y. Li, P. Hasin and Y. Wu, *Adv. Mater.*, 2010, **22**, 1926.
5 M. Yu, T. I. Draskovic and Y. Wu, *Phys. Chem. Chem. Phys.*, 2014, **16**, 5026.
6 J. Ahmed, C. K. Blakely, J. Prakash, S. R. Bruno, M. Yu, Y. Wu and V. V. Poltavets, *J. Alloys Compd.*, 2014, **591**, 275.
7 D. Xiong, Z. Xu, X. Zeng, W. Zhang, W. Chen, X. Xu, M. Wang and Y. B. Cheng, *J. Mater. Chem.*, 2012, 24760.
8 D. Xiong, W. Zhang, X. Zeng, Z. Xu, W. Chen, J. Cui, M. Wang, L. Sun and Y. B. Cheng, *ChemSusChem*, 2013, **6**, 1432.
9 Z. Xu, D. Xiong, H. Wang, W. Zhang, X. Zeng, L. Ming, W. Chen, X. Xu, J. Cui, M. Wang, S. Powar, U. Bach and Y.B. Cheng, *J. Mater. Chem. A*, 2014, **2**, 2968.
10 L. Alibabaei, H. Luo, R. L. House, P. G. Hoertz, R. Lopez and T. J. Meyer, *J. Mater. Chem. A*, 2013, **1**, 4133.
11 F. Li, K. Fan, B. Xu, E. Gabrielsson, Q. Daniel, L. Li and L. Sun, *J. Am. Chem. Soc.*, 2015, **137**, 9153.
12 K. Maeda and K. Domen, *J. Phys. Chem. Lett.*, 2010, **1**, 2655.
13 L. Alibabaei, M. K. Brennaman, M. R. Norris, B. Kalanyan, W. Song, M. D. Losego, J. J. Concepcion, R. A. Binstead, G. N. Parsons and T. J. Meyer, *Proc. Nat. Acad. Sci. USA*, 2013, **110**, 20008.
14 Z. Yu, F. Li and L. Sun, *Energy Environ. Sci.*, 2014, **8**, 760.
15 A. Nattestad, A. J. Mozer, M. K. R. Fischer, Y. Cheng, A. Mishra, P. Bäuerle and U. Bach, *Nat. Mater.*, 2009, **9**, 31.
16 C. C. Mercado, A. Zakutayev, K. Zhu, C. J. Flynn, J. F. Cahoon and A. J. Nozik, *J. Phys. Chem. C*, 2014, **118**, 25340.
17 J. D. Perkins, T. R. Paudel, A. Zakutayev, P. F. Ndione, P. A. Parilla, D. L. Young, S. Lany, D. S. Ginley, A. Zunger, N. H. Perry, Y. Tang, M. Grayson, T. O. Mason, J. S. Bettinger, Y. Shi and M. F. Toney, *Phys. Rev. B*, 2011, **84**, 1.
18 A. Zakutayev, T. R. Paudel, P. F. Ndione, J. D. Perkins, S. Lany, A. Zunger and D. S. Ginley, *Phys. Rev. B*, 2012, **85**, 1.
19 T. W. Kim, M. A. Woo, M. Regis and K. S. Choi, *J. Phys. Chem. Lett.*, 2014, **5**, 2370.
20 W. Luo, X. Hu, Y. Sun and Y. Huang, *J. Mater. Chem.*, 2012, **22**, 8916.
21 W. Wang, Y. Yang, S. Yang, Z. Guo, C. Feng and X. Tang, *Electrochim. Acta*, 2015, **155**, 297.
22 R. Wu, X. Qian, K. Zhou, J. Wei, J. Lou and P. M. Ajayan, *ACS Nano*, 2014, **8**, 6297.
23 Z. Ren, V. Botu, S. Wang, Y. Meng, W. Song, Y. Guo, R. Ramprasad, S. L. Suib and P.-X. Gao, *Angew. Chem. Int. Ed. Engl.*, 2014, **53**, 7223.
24 B. Liu, J. Zhang, X. Wang, G. Chen, D. Chen, C. Zhou and G. Shen, *Nano Lett.*, 2012, **12**, 3005–11.
25 L. Yan, T. Ren, X. Wang, Q. Gao, D. Ji and J. Suo, *Catal. Commun.*, 2003, **4**, 505.
26 T. Tsuzuki and P. McCormick, *J. Mater. Sci.*, 2004, **9**, 5143.
27 V. Šepelák, A. Düvel, M. Wilkening, K. D. Becker and P. Heitjans, *Chem. Soc. Rev.*, 2013, **42**, 7507.
28 W. M. Haynes, Ed., *CRC Handbook for Chemistry and Physics*, 96th edn.
29 S. Ito, T. N. Murakami, P. Comte, P. Liska, C. Grätzel, M. K. Nazeeruddin and M. Grätzel, *Thin Solid Films*, 2008, **516**, 4613.
30 A. Zakutayev, J. D. Perkins, P. A. Parilla, N. E. Widjonarko, A. K. Sigdel, J. J. Berry and D. S. Ginley, *MRS Commun.*, 2011, **1**, 23.
31 P. F. Ndione, Y. Shi, V. Stevanovic, S. Lany, A. Zakutayev, P. A. Parilla, J. D. Perkins, J. J. Berry, D. S. Ginley and M. F. Toney, *Adv. Funct. Mater.*, 2014, **24**, 610.
32 M. A. Chougule, S. G. Pawar, P. R. Godse, R. D. Sakhare, S. Sen and V. B. Patil, *J. Mater. Sci. Mater. Electron.*, 2012, **23**, 772.
33 Y. Kim, J. H. Lee, S. Cho, Y. Kwon, I. In, J. Lee, N. H. You, E. Reichmanis, H. Ko, K. T. Lee, H. K. Kwon, D. H. Ko, H. Yang and B. Park, *ACS Nano*, 2014, **8**, 6701.

Journal of Materials Chemistry A Accepted Manuscript

This journal is © The Royal Society of Chemistry 20xx

Please do not adjust margins

34 C. J. Flynn, E. E. Oh, S. M. McCullough, R. W. Call, C. L. Donley, R. Lopez and J. F. Cahoon, *J. Phys. Chem. C*, 2014, **118**, 14177.

35 E. Dell'Orto, L. Raimondo, A. Sassella and A. Abbotto, *J. Mater. Chem.*, 2012, **22**, 11364.

36 C. Pérez León, L. Kador, B. Peng and M. Thelakkat, *J. Phys. Chem. B*, 2006, **110**, 8723.

37 P. W. Atkins and J. de Paula, *Physical Chemistry*, 8th edn., 2006.

38 M. K. Nazeeruddin, E. Baranoff and M. Grätzel, *Sol. Energy*, 2011, **85**, 1172.

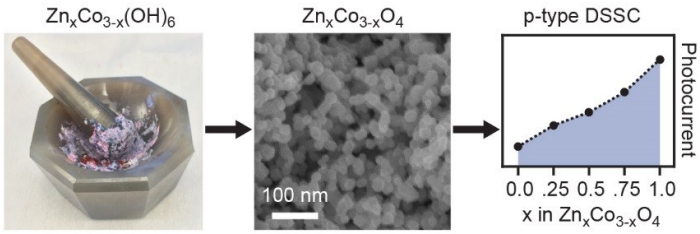

Table of contents figure

Journal of Materials Chemistry A Accepted Manuscript

Please do not adjust margins